High pressure synchrotron x-ray powder diffraction study of $Sc_2Mo_3O_{12}$ and $Al_2W_3O_{12}$

2005 J. Phys.: Condens. Matter 17 4271

(http://iopscience.iop.org/0953-8984/17/27/004)

INSTITUTE OF PHYSICS PUBLISHING JOURNAL OF PHYSICS: CONDENSED MATTER

J. Phys.: Condens. Matter **17** (2005) 4271–4283 doi:10.1088/0953-8984/17/27/004

High pressure synchrotron x-ray powder diffraction study of $Sc_2Mo_3O_{12}$ and $Al_2W_3O_{12}$

Tamas Varga[1], Angus P Wilkinson[1], Cora Lind[2], William A Bassett[3] and Chang-Sheng Zha[4]

[1] School of Chemistry and Biochemistry, Georgia Institute of Technology, Atlanta, GA 30332-0400, USA
[2] Department of Chemistry, The University of Toledo, Toledo, OH 43606-3390, USA
[3] Geological Sciences, Department of Earth and Atmospheric Sciences, Snee Hall, Cornell University, Ithaca, NY 14853-1504, USA
[4] CHESS, Wilson Laboratory, Cornell University, Ithaca, NY 14853, USA

Received 29 March 2005, in final form 7 June 2005
Published 24 June 2005
Online at stacks.iop.org/JPhysCM/17/4271

Abstract

Synchrotron x-ray powder diffraction was used to study $Sc_2Mo_3O_{12}$ and $Al_2W_3O_{12}$ at high pressure in a DAC. Both compounds adopt the orthorhombic $Sc_2W_3O_{12}$ structure under ambient conditions and exhibit anisotropic negative thermal expansion. A phase transition from orthorhombic ($Pnca$) to monoclinic ($P2_1/a$) symmetry was observed at ∼0.25 GPa for $Sc_2Mo_3O_{12}$ and at ∼0.1 GPa for $Al_2W_3O_{12}$ associated with a volume reduction of ∼1.5–2%. A second crystalline to crystalline phase transition was clearly seen only for $Sc_2Mo_3O_{12}$ (2.5–3.0 GPa). Peak broadening and almost complete amorphization were observed for $Sc_2Mo_3O_{12}$ at ∼8 GPa, and this was not fully reversible on decompression. At 7 GPa, the amorphization of $Al_2W_3O_{12}$ was not as advanced as for the molybdate and on decompression crystalline material was recovered. The compressibility of orthorhombic $Sc_2Mo_3O_{12}$ is highly anisotropic, but it is almost isotropic for both monoclinic $Sc_2Mo_3O_{12}$ and $Al_2W_3O_{12}$. Both compounds show a reduction in their bulk moduli (K_0) at the orthorhombic to monoclinic transition: 32(2) GPa for orthorhombic and 16(1) GPa for monoclinic $Sc_2Mo_3O_{12}$, and 48 GPa for orthorhombic and 28(1) GPa for monoclinic $Al_2W_3O_{12}$. $Sc_2Mo_3O_{12}$ displays very similar high pressure behaviour to the previously studied $Sc_2W_3O_{12}$.

1. Introduction

Materials exhibiting negative thermal expansion (NTE) have received considerable recent attention [1–6] due to a combination of academic interest and their potential for application in tailored thermal expansion composites [7–10]. Three families of compounds, AM_2O_8 (A = Zr, Hf and M = W or Mo), $A_2M_3O_{12}$ (A = a variety of 3+ ions, M = Mo or W) and AM_2O_7 (A = a variety of 4+ ions, M = P or V) have attracted the most interest. Their flexible

frameworks, relatively low densities and the presence of lattice modes that become softer on volume reduction [11–17] predispose these materials to rich behaviour upon the application of modest pressures, including crystalline to crystalline phase transitions [18–22] and pressure induced amorphization (PIA) [17, 19, 23, 24]. As phase transitions that occur at low pressure can be induced while processing, or using, composites that contain these materials, studies of high pressure behaviour have some practical as well as academic importance.

To date, there have been high pressure studies on the following members of the $A_2M_3O_{12}$ family of NTE compounds: $Sc_2W_3O_{12}$, $Sc_2Mo_3O_{12}$, $Al_2W_3O_{12}$, $Y_2W_3O_{12}$ and $Lu_2W_3O_{12}$ [25–36]. For $Sc_2Mo_3O_{12}$, crystalline to crystalline phase transitions have been reported at 0.3 and 2.7 GPa followed by PIA at ∼3.7 GPa on the basis of room temperature Raman and energy dispersive x-ray diffraction (EDXRD) data [31]. The amorphization was apparently initially reversible but became irreversible at higher pressures. The phase existing between 0.3 and 2.7 GPa was identified as monoclinic by comparison of the high pressure Raman spectra with those of the low temperature ambient pressure monoclinic form of $Sc_2Mo_3O_{12}$ [31]. In a combined Raman and XRD study of $Sc_2Mo_3O_{12}$ conducted by Arora *et al* [32] PIA was reported to occur in two stages beginning at 4 GPa with some disordering and ending at 12 GPa. In a very recent diffraction study, it was reported that the orthorhombic structure was maintained to ∼11 GPa [36] contrary to the findings of the earlier Raman work. A study examining samples of $Al_2W_3O_{12}$ that had been recovered from high temperature/pressure concluded that this compound undergoes no irreversible phase transitions below 8 GPa at room temperature and that at high pressure and temperature the material decomposes to form $AlWO_4$ [33]. AC resistivity and compressibility measurements at room temperature in large volume apparatuses were interpreted as indicating a reversible phase transition at 0.5 GPa [34]. In a Raman study of $Al_2(WO_4)_3$, reversible phase transitions were observed at 0.28 and 2.8 GPa [30]. The intermediate phase was identified as monoclinic. A recent diffraction study has confirmed the occurrence of two phase transitions at approximately these pressures on compression [37]. In a high pressure Raman and diffraction study of $Y_2W_3O_{12}$, a transformation of the ambient pressure orthorhombic phase to a disordered phase was seen at ∼3 GPa [35]. PIA has been reported to occur between 5 and 8 GPa at room temperature in $Lu_2(WO_4)_3$ samples recovered from high pressure using a multi-anvil device [25]. No other phase transformations were observed. Samples of $Sc_2W_3O_{12}$ recovered from room temperature and high pressure were examined by diffraction: irreversible PIA was observed to start at ∼5 GPa and be complete by ∼8 GPa [27]. Recently, we reported, on the basis of a monochromatic *in situ* synchrotron x-ray diffraction study, that $Sc_2W_3O_{12}$ showed two phase transitions on compression: one at ∼0.3 GPa giving a monoclinic phase and a second at ∼2.8 GPa leading to an unidentified phase [38]. The first phase transition was associated with a compressibility collapse similar to that seen in ReO_3 and NbO_2F [39–42]. The bulk modulus of the starting orthorhombic phase was estimated to be 31(3) GPa, but that for the monoclinic phase formed at 0.3 GPa was only 14(1) GPa.

In this paper, we present a high pressure *in situ* synchrotron diffraction study of $Sc_2(MoO_4)_3$ and $Al_2(WO_4)_3$ under (quasi)hydrostatic conditions in a diamond-anvil cell. These data, along with those from our recent study of $Sc_2W_3O_{12}$, allow us to look for chemical trends in the high pressure behaviour of compounds from the $A_2M_3O_{12}$ family.

2. Experimental details

2.1. Sample preparation

$Sc_2(MoO_4)_3$ powder was prepared from Sc_2O_3 (Strem Chemicals, Newburyport, MA) and MoO_3 (J T Baker, Phillipsburg, NJ). Stoichiometric amounts of the two oxides were thoroughly

mixed and ground. The mixture was initially heated at 700 °C for 5 h and after regrinding it was heated at 1100 °C for an additional 12 h in air.

$Al_2(WO_4)_3$ powder was synthesized from $Al_2O_3{\cdot}2H_2O$ (Catapal® B, a boehmite-type alumina, Vista Chemical Company, Houston, TX) and WO_3 (Aldrich, Milwaukee, WI). Stoichiometric amounts of the two oxides were thoroughly mixed and ground. The mixture was heated at 900, 1000 and 1100 °C for 20 h periods with intermittent grinding steps.

2.2. Diamond-anvil cells

A hydrothermal DAC (HDAC) [43, 44] was used with an anhydrous isopropanol pressure transmitting medium. This alcohol has been shown to provide hydrostatic pressure conditions up to 4.3 GPa [45]. For high pressure studies of this type, typically methanol:ethanol:water = 16:3:1 and methanol:ethanol = 4:1 with hydrostatic limits of 14.5 and 10.4 GPa, respectively, are used [45]. However, we chose not to use these media as water is known to react with some open-framework NTE materials including many members of the orthorhombic $A_2M_3O_{12}$ family [46–49] and cubic ZrW_2O_8 (resulting in a volume contraction) [50]. We have also seen evidence for a similar reaction between some NTE materials and methanol [51]. NaCl was used as a pressure calibrant. The diamonds were 1.7 mm thick with 500 μm culet faces. A rhenium gasket with a 300 μm hole diameter and 125 μm thickness was used. The gaskets were pre-indented between the diamonds. The downstream cone opening of the cell was 44° resulting in a $2\theta_{max}$ of 22° with ∼15° of usable data.

2.3. Diffraction data collection

Data were collected at room temperature and up to ∼8 GPa pressure for $Sc_2(MoO_4)_3$ and up to ∼7 GPa for $Al_2(WO_4)_3$ using the B-2 line of the Cornell High Energy Synchrotron Source (CHESS), Wilson Lab, Cornell University, Ithaca, NY. 25 keV (λ = 0.496 Å) x-rays were selected using a Ge(111) double-crystal monochromator. Diffraction patterns were recorded on imaging plates using 2–3 min exposures. The sample-to-plate distance was calibrated using diffraction from NaCl. For the purpose of this calibration a large amount of salt was packed on the outside face of one of the diamonds. The derived sample to plate distance was corrected for the thickness of the diamond (1.7 mm). This salt was removed after the sample to imaging plate calibration and a smaller amount of salt packed in the DAC with the sample ($A_2(MO_4)_3$:NaCl ∼ 2:3 ratio by weight) was used for pressure calibration.

2.4. Data analysis

The imaging plates were read using a BAS 2000 scanner and integrated to give intensity versus 2θ using the program SIMPA (v1.3) [52]. The integrated patterns were initially processed in JADE [53] for visualization and pressure calibration purposes. Further analysis was carried out by a combination of the Rietveld and Le Bail methods using GSAS [54].

Pressure was determined using the NaCl peak positions obtained by fitting in JADE and the program Calibration [55, 56]. The program Calibration makes use of the Birch equation of state for NaCl [56]. This equation of state is reported to be accurate to ∼1% in the range of our experiments [57, 58]. However, at low pressures the equation of state is not likely to be the dominant source of error in our pressure determination. We estimate a precision on our pressure measurements of ∼0.02 GPa, determined by the uncertainty in the NaCl peak position used for pressure calibration (∼0.001°) and the repeatability of DAC positioning between measurements, along with, at low pressures, a possible error of ∼0.05 GPa primarily

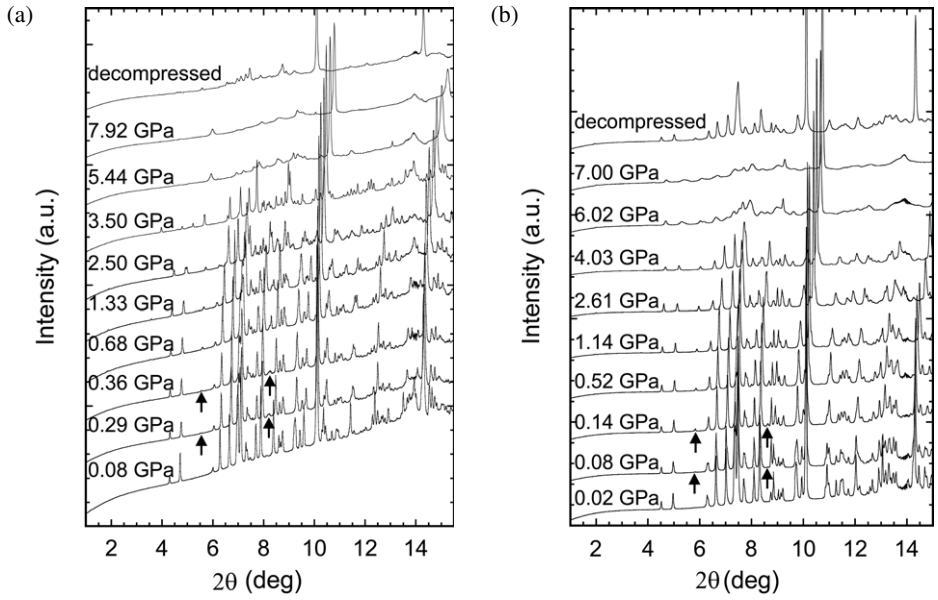

Figure 1. Powder diffraction patterns as a function of pressure for (a) $Sc_2Mo_3O_{12}$ and (b) $Al_2W_3O_{12}$. Arrows indicate the location of peaks that are characteristic of the monoclinic phase. The data were collected at 25 keV ($\lambda = 0.496$ Å).

due to inaccuracies in the calibration of the sample to image plate distance due to uncertainties in the thickness of the diamonds and the NaCl layer on the outer face of the diamond that was used for DAC to image plate distance calibration.

As the pressure was increased, diffraction data were collected at each pressure point. Le Bail fits were carried out to extract the lattice parameters at each pressure. In these fits, only the lattice parameters and profile parameters were varied. For the pressures where there was evidence for the coexistence of orthorhombic and monoclinic phases, the Rietveld method was used to obtain an estimate of the amount of each phase that was present. In these fits, the lattice parameters for each phase, the background terms, the scale factors and the peak profile parameters were optimized, but the structural models were not refined due to the limited amount of data (low Q_{max}) available. Structural models for these fits were obtained from Abrahams and Bernstein [59] (orthorhombic model) as well as Evans and Mary [60] ($Sc_2Mo_3O_{12}$ monoclinic model). The calculated unit cell volumes were fitted to the Birch–Murnaghan equation of state (EOS) [61] using the EOS-FIT program (v5.2) [62]. The third-order Birch–Murnaghan EOS was used for both the orthorhombic and monoclinic phases.

3. Results

3.1. $Sc_2Mo_3O_{12}$

A selection of the recorded diffraction patterns for $Sc_2Mo_3O_{12}$ is shown in figure 1(a), along with data for $Al_2W_3O_{12}$ in figure 1(b). The diffraction data for the molybdate are consistent with a transition from the ambient pressure and temperature orthorhombic structure (space group: $Pnca$) to a monoclinic structure (space group: $P2_1/a$) at around 0.25 GPa. At ambient pressure this monoclinic structure is only seen for $Sc_2Mo_3O_{12}$ at low temperatures (<180 K) [60, 63, 64]. Rietveld fits to the diffraction patterns indicate the onset of this transition is at ∼0.25 GPa, with

Table 1. $Sc_2(MoO_4)_3$ lattice constants as a function of pressure. Derived pseudo-orthorhombic values are given for the monoclinic phase along with the primitive monoclinic lattice constants that were directly determined from the diffraction data. The wt% of the two $Sc_2Mo_3O_{12}$ phases, as estimated by Rietveld analysis, in the mixed phase samples is given. The balance of the sample is NaCl.

Pressure (GPa)	Symmetry	a (Å)	b (Å)	c (Å)	β or α (deg)	Volume (Å^3)
0.08	Orthorhombic	9.6305(4)	13.2271(6)	9.5368(4)	90.000	1214.83(12)
0.12	Orthorhombic	9.6262(3)	13.2252(4)	9.5345(3)	90.000	1213.82(8)
0.18	Orthorhombic	9.6254(3)	13.2078(5)	9.5303(3)	90.000	1211.58(9)
0.24 39.7%	Orthorhombic	9.6199(5)	13.1928(7)	9.5267(5)	90.000	1209.07(14)
3.6%	Monoclinic	—	—	—	—	
0.29 24.3%	Orthorhombic	9.5468(7)	13.1777(10)	9.4240(7)	90.000	1185.58(11)
	Pseudo-ortho	9.5405	13.1734	9.4219	89.67	
21.1%	Monoclinic	16.1513(3)	9.5405(4)	18.8438(6)	125.352(2)	2368.26(7)
0.36 21.4%	Orthorhombic	9.5261(15)	13.1718(16)	9.4025(14)	90.000	1179.79(20)
	Pseudo-ortho	9.5191	13.1540	9.3950	89.71	
23.3%	Monoclinic	16.1263(7)	9.5191(4)	18.7900(9)	125.346(2)	2352.76(11)
0.60 4.4%	Orthorhombic	—	—	—	—	
	Pseudo-ortho	9.4752	13.0984	9.3486	89.65	2320.48(13)
39.3%	Monoclinic	16.0460(6)	9.4752(3)	18.6973(6)	125.285(1)	
0.68	Monoclinic	16.0141(6)	9.4602(3)	18.6586(6)	125.266(1)	2307.96(13)
	Pseudo-ortho	9.4602	13.0754	9.3293	89.64	
0.86	Monoclinic	15.9587(8)	9.4306(3)	18.5977(8)	125.219(2)	2286.63(18)
	Pseudo-ortho	9.4306	13.0378	9.2988	89.58	
1.15	Monoclinic	15.8750(7)	9.3877(4)	18.5124(8)	125.184(2)	2254.86(18)
	Pseudo-ortho	9.3877	12.9752	9.2562	89.52	
1.33	Monoclinic	15.8175(12)	9.3588(5)	18.4553(15)	125.153(3)	2233.71(30)
	Pseudo-ortho	9.3588	12.9332	9.2276	89.47	
1.63	Monoclinic	15.7475(6)	9.3193(3)	18.3893(8)	125.130(2)	2207.16(16)
	Pseudo-ortho	9.3193	12.8798	9.1946	89.41	
1.84	Monoclinic	15.6948(7)	9.2906(3)	18.3435(9)	125.108(2)	2188.15(19)
	Pseudo-ortho	9.2906	12.8402	9.1718	89.35	
2.20	Monoclinic	15.5944(7)	9.2094(4)	18.2611(9)	125.106(3)	2145.50(9)
	Pseudo-ortho	9.2094	12.7586	9.1306	89.27	
2.50	Monoclinic	15.4668(13)	9.1104(7)	18.1547(14)	124.743(3)	2102.08(32)
	Pseudo-ortho	9.1104	12.7120	9.0774	88.82	

an approximate 50:50 mix of orthorhombic and monoclinic material in the 0.3–0.35 GPa range and almost complete transformation to monoclinic material by 0.6 GPa. A second transition giving a phase with unidentified symmetry was observed at ∼2.5 GPa. Further compression to ∼7.9 GPa resulted in considerable peak broadening and a very weak diffraction pattern, but not complete amorphization. Decompression at ambient temperature did not lead to recovery of the starting orthorhombic phase; some weak Bragg peaks were seen from the decompressed material, but they were not readily assignable as arising from any of the crystalline phases that were observed on compression.

Lattice constants for the orthorhombic and monoclinic phases, derived from Le Bail fits to the data using GSAS, are shown as a function of pressure in table 1. As the structures of the monoclinic and orthorhombic phases are very closely related to one another [60] it is possible

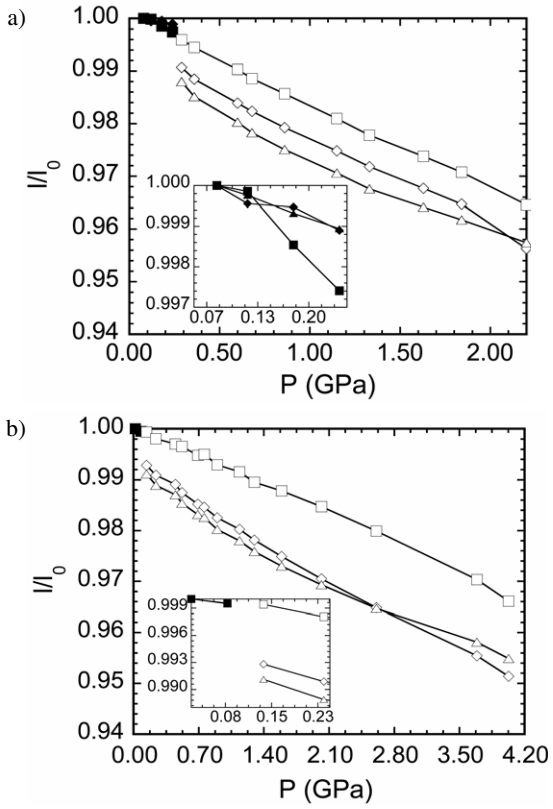

Figure 2. Normalized lattice constants as a function of pressure for (a) $Sc_2Mo_3O_{12}$ and (b) $Al_2W_3O_{12}$. These data are normalized to the lowest pressure point, not zero pressure. The monoclinic lattice constants have been converted to pseudo-orthorhombic values. The insets show the low pressure orthorhombic regions. The lines are only a guide to the eye. Solid diamonds: a/a_0 orthorhombic, solid squares: b/b_0 orthorhombic, solid triangles: c/c_0 orthorhombic, open diamonds: a/a_0 monoclinic, open squares: b/b_0 monoclinic, open triangles: c/c_0 monoclinic.

to transform the primitive monoclinic lattice constants to a new A-centred monoclinic lattice that is pseudo-orthorhombic with $a_m \sim a_o$, $b_m \sim 2c_o$, $c_m \sim 2b_o$ and $\alpha_m \sim 90°$ using the matrix (0 1 0; 0 0 −1; −2 0 −1) so that changes in linear compressibility through the phase transformation can be examined. The transformed pseudo-orthorhombic lattice constants for the monoclinic phase are also shown in table 1, and both the orthorhombic and pseudo-orthorhombic values are plotted in figures 2 and 3. The orthorhombic phase displays highly anisotropic compressibility, with the b-axis much softer ($\beta_b = 1.7(2) \times 10^{-2}$ GPa^{-1}) than the a- and c-axes ($\beta_a = 6(1) \times 10^{-3}$ GPa^{-1} and $\beta_c = 6.7(2) \times 10^{-3}$ GPa^{-1}, respectively). The b-axis varies almost continuously through the phase transition, but there is a sharp discontinuity on the a- and c-axes associated with a pronounced softening in these directions at the phase transition. The monoclinic phase displays almost isotropic compressibility. The corresponding linear compressibilities are: $\beta_a = 1.73(4) \times 10^{-2}$ GPa^{-1}, $\beta_b = 1.65(3) \times 10^{-2}$ GPa^{-1} and $\beta_c = 1.60(8) \times 10^{-2}$ GPa^{-1}. The variation of normalized volume with pressure is shown in figure 4. There is a <1% decrease in volume prior to the phase transition and a 1.5–2% decrease at the transition itself. Fitting an EOS to the volume data gave a bulk modulus (K_0) of 32(2) GPa for the orthorhombic and 16(1) GPa for the monoclinic phase, indicating

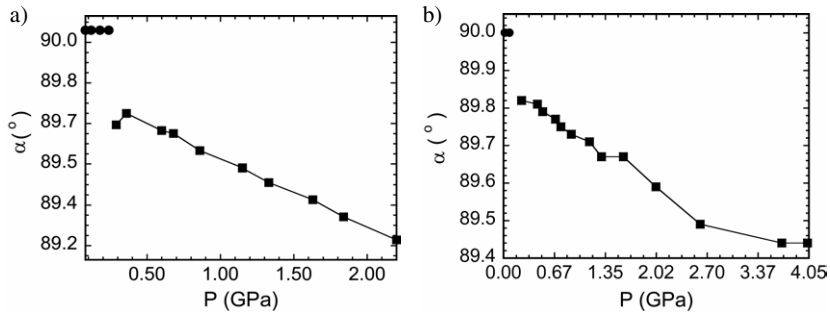

Figure 3. Orthorhombic and pseudo-orthorhombic angles alpha as a function of pressure for (a) $Sc_2Mo_3O_{12}$ and (b) $Al_2W_3O_{12}$. The lines are only a guide to the eye. Circles: orthorhombic, squares: monoclinic.

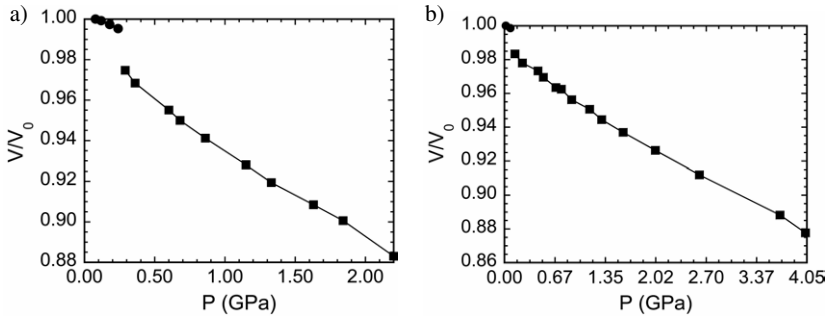

Figure 4. Normalized unit cell volume as a function of pressure for (a) $Sc_2Mo_3O_{12}$ and (b) $Al_2W_3O_{12}$. Circles: orthorhombic, squares: monoclinic. These data are normalized to the lowest pressure point, not zero pressure.

that, like $Sc_2W_3O_{12}$, $Sc_2Mo_3O_{12}$ displays an unusual softening on going through the phase transition [38]. The pressure derivatives were 4.0 (implied value) and 4(1); the zero-pressure volumes were 304.43(10) Å^3 and 300.71(77) Å^3 (per formula unit), respectively.

3.2. $Al_2W_3O_{12}$

A selection of the diffraction patterns recorded for $Al_2W_3O_{12}$ is shown in figure 1(b). The data are consistent with a transition from the ambient pressure and temperature orthorhombic structure ($Pnca$) to a monoclinic structure ($P2_1/a$) at ∼0.1 GPa. At ambient pressure this monoclinic structure forms on cooling to <267 K [63]. Rietveld fits to the diffraction patterns indicate that the onset of this transition is at <0.08 GPa, with an approximate 3:2 mix of orthorhombic and monoclinic material by 0.14 GPa, and complete transformation to monoclinic material at <0.24 GPa. Unlike those for $Sc_2Mo_3O_{12}$, the diffraction data do not clearly indicate any further crystalline to crystalline phase transitions, although above 4 GPa the peak broadening is sufficiently great that changes could be easily obscured. By 7.0 GPa the diffraction data showed only weak broad peaks but on decompression the quality of the diffraction pattern improved dramatically and showed well defined Bragg peaks; the peak broadening is slightly more pronounced in this pattern than in those collected during the initial compression. The data are consistent with the recovery of the monoclinic, not the starting

Table 2. $Al_2(WO_4)_3$ lattice constants as a function of pressure. Derived pseudo-orthorhombic values are given for the monoclinic phase along with the primitive monoclinic lattice constants that were directly determined from the diffraction data. The wt% of the two $Al_2W_3O_{12}$ phases, as estimated by Rietveld analysis, in the mixed phase samples is given. The balance of the sample is NaCl.

Pressure (GPa)	Symmetry	a (Å)	b (Å)	c (Å)	β or α (deg)	Volume (Å^3)
0.02	Orthorhombic	9.1367(3)	12.5940(4)	9.0553(3)	90.000	1041.97(5)
0.08 24.7%	Orthorhombic	9.1325(4)	12.5877(6)	9.0505(4)	90.000	1040.42(10)
	Pseudo-ortho	9.0722	12.5949	8.9787	89.79	
10.8%	Monoclinic	15.4406(15)	9.0722(6)	17.9574(17)	125.344(6)	2051.85(22)
0.14 19.4%	Orthorhombic	9.0710(5)	12.5872(7)	8.9736(5)	90.000	1024.59(6)
	Pseudo-ortho	9.0710	12.5864	8.9749	89.73	
13.0%	Monoclinic	15.4244(15)	9.0710(7)	17.9498(15)	125.314(7)	2049.33(16)
0.24	Monoclinic	15.4098(16)	9.0533(5)	17.9093(12)	125.346(5)	2037.97(26)
	Pseudo-ortho	9.0533	12.5694	8.9546	89.82	
0.45	Monoclinic	15.3884(13)	9.0370(5)	17.8756(12)	125.318(4)	2028.35(23)
	Pseudo-ortho	9.0370	12.5564	8.9378	89.81	
0.52	Monoclinic	15.3719(12)	9.0218(6)	17.8454(13)	125.272(5)	2020.51(24)
	Pseudo-ortho	9.0218	12.5500	8.9227	89.79	
0.69	Monoclinic	15.3401(11)	9.0013(5)	17.8050(11)	125.245(4)	2007.85(21)
	Pseudo-ortho	9.0013	12.5282	8.9025	89.77	
0.76	Monoclinic	15.3368(11)	8.9957(5)	17.7943(12)	125.211(4)	2005.79(22)
	Pseudo-ortho	8.9957	12.5308	8.8972	89.75	
0.90	Monoclinic	15.3013(12)	8.9767(5)	17.7522(13)	125.191(4)	1992.71(24)
	Pseudo-ortho	8.9767	12.5049	8.8761	89.73	
1.14	Monoclinic	15.2728(10)	8.9561(5)	17.7120(11)	125.152(4)	1980.90(21)
	Pseudo-ortho	8.9561	12.4876	8.8560	89.71	
1.30	Monoclinic	15.2350(9)	8.9367(4)	17.6732(11)	125.122(3)	1968.10(20)
	Pseudo-ortho	8.9367	12.4614	8.8366	89.67	
1.59	Monoclinic	15.2027(10)	8.9072(5)	17.6210(11)	125.088(3)	1952.48(21)
	Pseudo-ortho	8.9072	12.4401	8.8105	89.67	
2.02	Monoclinic	15.1416(11)	8.8669(6)	17.5549(14)	125.017(4)	1930.26(25)
	Pseudo-ortho	8.8669	12.4010	8.7774	89.59	
2.61	Monoclinic	15.0555(9)	8.8153(5)	17.4710(10)	124.952(4)	1900.50(11)
	Pseudo-ortho	8.8153	12.3404	8.7355	89.49	
3.69	Monoclinic	14.9174(9)	8.7292(5)	17.3516(8)	124.998(4)	1850.90(9)
	Pseudo-ortho	8.7292	12.2205	8.6758	89.44	
4.03	Monoclinic	14.8572(11)	8.6925(5)	17.2936(12)	125.027(6)	1828.87(10)
	Pseudo-ortho	8.6925	12.1668	8.6468	89.44	
Decompr.	Monoclinic	15.420(15)	9.0444(10)	17.9205(23)	125.288(67)	2039.99
0.18	*Pseudo-ortho*	9.0444	12.5868	8.9602	89.76	

orthorhombic, structure and NaCl peak positions for this sample indicate a residual pressure of ∼0.18 GPa.

Lattice constants for the orthorhombic and monoclinic phases, derived from Le Bail fits to the data using GSAS, are shown as a function of pressure in table 2 along with pseudo-orthorhombic values for the monoclinic phase that were derived by transformation as described for $Sc_2Mo_3O_{12}$ in the previous section. The orthorhombic and pseudo-orthorhombic values are plotted in figures 2 and 3.

As we have only one data set at pressures where only the orthorhombic phase was present (0.02 GPa) and a further data set at a pressure where the orthorhombic phase is dominant (0.08 GPa), there are insufficient data for a high quality determination of linear compressibilities for the orthorhombic phase. Our best estimates based on only two data points are: $\beta_a = 7.66 \times 10^{-3}$ GPa^{-1}, $\beta_b = 8.34 \times 10^{-3}$ GPa^{-1} and $\beta_c = 8.84 \times 10^{-3}$ GPa^{-1}. The orthorhombic lattice constants from the 0.14 GPa data appear to be in error, probably due to correlations between the lattice constants of the closely related monoclinic and orthorhombic structures. On the basis of the limited data that is available, the anisotropy in the compressibility appears to be less than that for $Sc_2Mo_3O_{12}$. In figure 2(b) we can see that the *b*-axis varies in an almost continuous fashion through the phase transition, but there is a sharp discontinuity on both the *a*- and *c*-axes associated with the phase transition. The monoclinic phase displays almost isotropic compressibility (with linear compressibilities of: $\beta_a = 1.07(2) \times 10^{-2}$ GPa^{-1}, $\beta_b = 8.4(1) \times 10^{-3}$ GPa^{-1} and $\beta_c = 9.3(4) \times 10^{-3}$ GPa^{-1}); there is an apparent softening at >2.6 GPa (see also figure 4) that may indicate a phase transition that is not clearly seen in the raw diffraction data. The variation of normalized volume with pressure is shown in figure 4. There is a volume decrease at the orthorhombic–monoclinic phase transition of ∼1.5%. Fitting an EOS to the volume data gave a bulk modulus (K_0) of 48 GPa for the orthorhombic (based on only two points) and 28(1) GPa for the monoclinic phase. The pressure derivatives were 4.0 (implied value) and 3.7(7), and the zero-pressure volumes were 260.61 and 257.14(28) Å^3 per formula unit, for the orthorhombic and monoclinic phases respectively. These data suggest that, like $Sc_2W_3O_{12}$ and $Sc_2Mo_3O_{12}$, $Al_2W_3O_{12}$ becomes softer on going through the phase transition.

4. Discussion

The phase transition pressures seen for $Sc_2Mo_3O_{12}$ in our monochromatic diffraction study (∼0.25 and ∼2.5 GPa) are in reasonable agreement with those previously reported for this compound on the basis of Raman and EDXRD data (0.3 and 2.7 GPa) [31] and they are close to those observed in our previous study of $Sc_2W_3O_{12}$ (0.3 and 2.8 GPa) [38]. However, these results are contrary to those of a recent high pressure diffraction study of $Sc_2Mo_3O_{12}$, that reported no transitions below 11 GPa [36]. This discrepancy may be due to the relatively low resolution of the diffraction data in the study of Arora *et al* [36]. Comparison of the diffraction data for the phase formed at >2.4 GPa with the corresponding data for $Sc_2W_3O_{12}$ [38] suggests that this, as yet unidentified phase has the same structure as the corresponding tungstate. The bulk moduli for the orthorhombic and monoclinic forms of $Sc_2Mo_3O_{12}$ (32(2) and 16(1) GPa, respectively) are also very close to those that we previously determined for $Sc_2W_3O_{12}$ (31(3) and 14(1) GPa, respectively). The anisotropy of the compressibility that is seen in orthorhombic $Sc_2Mo_3O_{12}$ is also seen in the corresponding tungstate [38]. Clearly, the replacement of tungsten by molybdenum in $Sc_2W_3O_{12}$ leads to little change in the high pressure properties of the material, even though at ambient pressure the two compounds have markedly different temperatures for their ferroelastic orthorhombic to monoclinic phase transitions [63]; the tungstate does not undergo this transition above 10 K [65], but the molybdate undergoes this transition at 180 K [60]. The behaviour of the orthorhombic/pseudo-orthorhombic lattice constants on compression for the two scandium compounds is also very similar with sharp discontinuities in the *a* and *c* lattice constants, but an almost continuous variation on the *b*-axis through the transition (figure 2(a), table 1). Interestingly, similar behaviour is seen for $Sc_2Mo_3O_{12}$ at ambient pressure as the temperature is varied (see figure 5) [60]; there is a 0.15% increase in the *b*-axis length on cooling through the transition to get monoclinic material, but decreases of nearly 1% for the *a*- and *c*-axes. The overall volume decrease (1.5%) associated

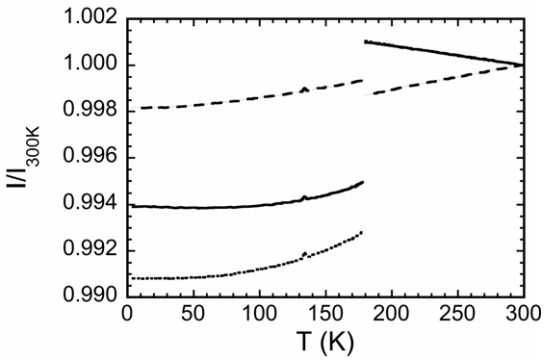

Figure 5. Normalized lattice constants for $Sc_2Mo_3O_{12}$ as a function of temperature, at ambient pressure, for comparison with their behaviour under pressure (figure 2). The monoclinic lattice constants are expressed in pseudo-orthorhombic form. The solid, long dashed and short dashed lines are the normalized *a*-, *b*-and *c*-axis lengths respectively. The monoclinic to orthorhombic phase transition at ∼178 K is clearly visible. Note that the lines for the orthorhombic *a* and *c* lattice constants overlap with one another. These data were kindly provided by John S O Evans.

with the thermally induced transition is similar to that seen for the pressure induced transition. As previously pointed out for the tungstate [38], the structural changes accompanying volume reduction on compression of the orthorhombic phase must be different from those involved in the volume reduction that occurs on heating at ambient pressure as the *a*- and *c*-axes have negative coefficients of thermal expansion (CTE), but the *b*-axis has a positive CTE [60], whereas all axis lengths decrease on compression.

The behaviour of $Al_2W_3O_{12}$ on compression is different from that of both $Sc_2W_3O_{12}$ and $Sc_2Mo_3O_{12}$. The orthorhombic to monoclinic transformation is seen at lower pressure (onset ∼0.1 GPa) for the aluminium compound than for the scandium compounds, although in a previous Raman study it was reported to occur at 0.28 GPa [30], and a second crystalline to crystalline phase transition, analogous to those seen at ∼2.6 GPa in the two scandium compounds, is not observed; there are no major changes in the powder diffraction patterns of $Al_2W_3O_{12}$ in the pressure range 0.15–4.0 GPa. However, a prior Raman study of this compound indicated that there was a second transition at 2.8 GPa [30] and the occurrence of a second transition has also been suggested on the basis of prior diffraction measurements [37]. Careful inspection of the lattice constants and unit cell volumes derived from our study (see figures 2(b) and 4(b)) reveals an unexpected softening above 2.6 GPa that is coincident with a change in the pressure dependence of the monoclinic angle (figure 3(b)). These changes may be an indication of a transition that has only subtle effects on the diffraction pattern. In the prior high pressure Raman study of $Al_2(WO_4)_3$ [30], it was stated that the phase existing above 2.8 GPa probably contained WO_4 tetrahedra with smaller distortions than those in the MoO_4 tetrahedra of $Sc_2Mo_3O_{12}$ at pressures above 2.7 GPa; this is consistent with our observation of an obvious structural change in the molybdate but no obvious change in the case of $Al_2W_3O_{12}$.

The phase coexistence that is associated with the pressure induced orthorhombic to monoclinic transitions in both $Sc_2Mo_3O_{12}$ and $Al_2W_3O_{12}$ suggests that there is hysteresis associated with the transition. This introduces uncertainty into the estimation of the true thermodynamic phase transition pressure from our data. However, the onset pressures for the transitions observed in our measurements (<0.1 GPa for $Al_2W_3O_{12}$, <0.24 GPa for $Sc_2Mo_3O_{12}$ and <0.28 GPa for $Sc_2W_3O_{12}$ [38]) are consistent with the rationalization that was put forward by Sleight [63, 64] for the composition dependence of the orthorhombic–

monoclinic phase transition temperature at ambient pressure within the series of molybdates or tungstates. He argued that as the electronegativity of the A^{3+} cation increases (aluminium is more electronegative than scandium), there is less negative charge on the oxide ions and consequently less repulsion between oxide ions resisting a volume collapse giving the monoclinic structure at higher temperatures. On the basis of this argument we would expect a lower phase transition pressure for $Al_2W_3O_{12}$ than for $Sc_2W_3O_{12}$.

The available, somewhat limited, diffraction data suggest that orthorhombic $Al_2W_3O_{12}$ does not have a strongly anisotropic compressibility in contrast to what is seen for the scandium compounds and to the large anisotropy of the thermal expansion seen for $Al_2W_3O_{12}$; the thermal expansion coefficients determined from a single crystal by dilatometry are $\alpha_a = -1.69 \times 10^{-6}\,^{\circ}C^{-1}$, $\alpha_b = 8.31 \times 10^{-6}\,^{\circ}C^{-1}$ and $\alpha_c = -0.15 \times 10^{-6}\,^{\circ}C^{-1}$ [66].

While the estimated bulk modulus for orthorhombic $Al_2W_3O_{12}$ (∼48 GPa) is somewhat uncertain due to the limited amount of data that were available at very low pressure (only two data points), it is considerably larger than those for $Sc_2Mo_3O_{12}$ and $Sc_2W_3O_{12}$ (32(2) and 31(3) GPa, respectively). Additionally, the bulk modulus of the monoclinic aluminium tungstate, 28(1) GPa, is also much larger than those for the two scandium compounds (16(1) GPa for the molybdate and 14(1) GPa for the tungstate). The considerable increase in bulk modulus on going from the scandium compounds to aluminium tungstate can be rationalized by considering the packing densities of the different compounds; at ambient temperature and pressure, each oxygen in the orthorhombic scandium molybdate occupies a volume of ∼25.5 Å^3 [60], but for $Al_2W_3O_{12}$, the volume per oxygen is only ∼21.6 Å^3 [33]. The greater oxygen packing density in the aluminium compound will lead to more oxygen–oxygen repulsion on compression and a higher bulk modulus. The packing density in the monoclinic aluminium compound is also much higher than that in monoclinic scandium molybdate, so a similar rationalization of their relative bulk moduli can be used. However, this simplistic rationalization does not seem to be entirely consistent with Sleight's explanation [63, 64] for the composition dependence of the orthorhombic–monoclinic phase transition temperature at ambient pressure within the series of molybdates or tungstates that was mentioned in the previous paragraph. A comprehensive understanding of how changes in A^{3+} influence the phase transition temperatures and pressures, and the compressibilities of both the orthorhombic and monoclinic phases can probably only be achieved by considering entropic as well as enthalpic factors. There is presumably a significant loss of vibrational entropy on going from the orthorhombic to the monoclinic phase and this entropy change will be dependent on the identity of A^{3+}, as the nature of this cation can affect the unit cell volume quite dramatically and hence change the phonon density of states.

There has been considerable recent discussion of pressure induced amorphization (PIA) in NTE materials; see for example the recent paper of Sikka [67]. Our diffraction data show marked line broadening at pressures above ∼4 GPa that might be associated with PIA and, in the case of the $Sc_2Mo_3O_{12}$, the diffraction pattern did not recover on decompression. However, the pressure transmitting medium that we employed, anhydrous isopropanol, is not hydrostatic above 4.3 GPa and the high pressure effects that we observe may be a consequence of the sample's stress state rather than an intrinsic disordering that would be seen even under hydrostatic conditions.

5. Conclusions

The replacement of tungsten in $Sc_2W_3O_{12}$ by molybdenum to give $Sc_2Mo_3O_{12}$ leads to no major changes in the high pressure behaviour of the material. The nature of the high pressure phases that occur, the transition pressures and their compressibilities are almost the same.

However, $Al_2W_3O_{12}$ displays quite different high pressure behaviour. The phase that appears on compression of either of the scandium compounds to ∼2.6 GPa is not formed on compression of the aluminium compound, and the bulk moduli for monoclinic $Al_2W_3O_{12}$, and probably the orthorhombic phase as well, are much higher than those for the corresponding scandium tungstate and molybdate phases. $Sc_2Mo_3O_{12}$, $Sc_2W_3O_{12}$ and, probably, $Al_2W_3O_{12}$ show a softening at their orthorhombic to monoclinic transition pressures; the bulk modulus of the high pressure phase is less than that of the low pressure phase.

Acknowledgments

This work is based upon research conducted at the Cornell High Energy Synchrotron Source (CHESS) which is supported by the National Science Foundation and the National Institutes of Health/National Institute of General Medical Sciences under award DMR-0225180. APW is grateful for support under National Science Foundation grant DMR-0203342. The authors thank John S O Evans for providing the thermal expansion data on $Sc_2Mo_3O_{12}$. We are grateful to Mehmet Cetinkol for the preparation of the $Al_2W_3O_{12}$.

References

[1] Sleight A W 1995 *Endeavour* **19** 64
[2] Sleight A W 1998 *Inorg. Chem.* **37** 2854
[3] Sleight A W 1998 *Annu. Rev. Mater. Sci.* **28** 29
[4] Sleight A W 1998 *Curr. Opin. Solid State Mater. Sci.* **3** 128
[5] Evans J S O, Mary T A and Sleight A W 1998 *Physica* B **241–243** 311
[6] Evans J S O 1999 *J. Chem. Soc. Dalton Trans.* 3317
[7] Wetherfold R C and Wang J 1995 *Compos. Sci. Technol.* **53** 1
[8] Fleming D A, Johnson D W and Lemaire P J 1997 *US Patent Specification* 5,694,503 (Lucent Technologies, USA)
[9] Fleming D A, Lemaire P J and Johnson D W 1998 *European Patent Specification* EP 97-306798 19970902 (Lucent Technologies, Inc., USA)
[10] Balch D K and Dunand D C 2004 *Metall. Mater. Trans.* A **35** 1159
[11] Mittal R, Chaplot S L, Kolesnikov A I, Loong C-K and Mary T A 2003 *Phys. Rev.* B **68** 054302
[12] Mittal R, Chaplot S L, Schober H and Mary T A 2001 *Phys. Rev. Lett.* **86** 4692
[13] Mittal R, Chaplot S L, Schober H, Kolesnikov A I, Loong C-K, Lind C and Wilkinson A P 2004 *Phys. Rev.* B **70** 214303
[14] Ravindran T R, Arora A K and Mary T A 2000 *Phys. Rev. Lett.* **84** 3879
[15] Ravindran T R, Arora A K and Mary T A 2001 *J. Phys.: Condens. Matter* **13** 11573
[16] Yamamura Y, Nakajima N, Tsuji T, Koyano M, Iwasa Y, Katayama S, Saito K and Sorai M 2002 *Phys. Rev.* B **66** 014301
[17] Chen B, Muthu D V S, Liu Z X, Sleight A W and Kruger M B 2001 *Phys. Rev.* B **64** 214111
[18] Evans J S O, Hu Z, Jorgensen J D, Argyriou D N, Short S and Sleight A W 1997 *Science* **275** 61
[19] Grzechnik A and Crichton W A 2002 *Solid State Sci.* **4** 1137
[20] Grzechnik A, Crichton W A, Syassen K, Adler P and Mezouar M 2001 *Chem. Mater.* **13** 4255
[21] Jorgensen J D, Hu Z, Short S, Sleight A W and Evans J S O 2001 *J. Appl. Phys.* **89** 3184
[22] Jorgensen J D, Hu Z, Teslic S, Argyriou D N, Short S, Evans J S O and Sleight A W 1999 *Phys. Rev.* B **59** 215
[23] Perottoni C A and de Jornada J A H 1998 *Science* **280** 886
[24] Lind C, VanDerveer D G, Wilkinson A P, Chen J, Vaughan M T and Weidner D J 2001 *Chem. Mater.* **13** 487
[25] Liu H, Secco R A, Imanaka N and Adachi G 2002 *Solid State Commun.* **121** 177
[26] Secco R A 2002 *Recent Res. Dev. Non-Cryst. Solids* **2** 171
[27] Secco R A, Liu H, Imanaka N and Adachi G 2001 *J. Mater. Sci. Lett.* **20** 1339
[28] Secco R A, Liu H, Imanaka N and Adachi G 2002 *J. Phys.: Condens. Matter* **14** 11285
[29] Secco R A, Liu H, Imanaka N, Adachi G and Rutter M D 2002 *J. Phys. Chem. Solids* **63** 425
[30] Maczka M, Paraguassu W, Souza Filho A G, Freire P T C, Mendes Filho J, Melo F E A and Hanuza J 2004 *J. Solid State Chem.* **177** 2002

[31] Paraguassu W, Maczka M, Souza Filho A G, Freire P T C, Mendes Filho J, Melo F E A, Macalik L, Gerward L, Staun Olsen J, Waskowska A and Hanuza J 2004 *Phys. Rev.* B **69** 094111
[32] Arora A K, Nithya R, Yagi T, Miyajima N and Mary T A 2004 *Solid State Commun.* **129** 9
[33] Achary S N, Mukherjee G D, Tyagi A K and Vaidya S N 2002 *J. Mater. Sci.* **37** 2501
[34] Mukherjee G D, Achary S N, Tyagi A K and Vaidya S N 2003 *J. Phys. Chem. Solids* **64** 611
[35] Karmakar S, Deb S K, Tyagi A K and Sharma S M 2004 *J. Solid State Chem.* **177** 4087
[36] Arora A K, Yagi T, Miyajima N and Mary T A 2005 *J. Appl. Phys.* **97** 013508
[37] Mukherjee G D, Vijaykumar V, Achary S N, Tyagi A K and Godwal B K 2004 *J. Phys.: Condens. Matter* **16** 7321
[38] Varga T, Wilkinson A P, Lind C, Bassett W A and Zha C-S 2005 *Phys. Rev.* B at press
[39] Batlogg B, Maines R G, Greenblatt M and DiGregorio S 1984 *Phys. Rev.* B **29** 3762
[40] Jorgensen J-E, Jorgensen J D, Batlogg B, Remeika J P and Axe J D 1986 *Phys. Rev.* B **33** 4793
[41] Carlson S 2000 *J. Appl. Crystallogr.* **33** 1175
[42] Carlson S, Larsson A-K and Rohrer F E 2000 *Acta Crystallogr.* B **56** 189
[43] Bassett W A, Shen A H, Bucknum M and Chou I-M 1993 *Rev. Sci. Instrum.* **64** 2340
[44] Bassett W A, Anderson A J, Mayanovic R A and Chou I-M 2000 *Chem. Geol.* **167** 3
[45] Miletich R, Allan D R and Kuhs W F 2001 *Rev. Mineral. Geochem.* **41** 445
[46] Nassau K, Levinstein H J and Loiacono G M 1965 *J. Phys. Chem. Solids* **26** 1805
[47] Avzhieva E M, Shakhno I V, Plyushchev V E, Voronskaya G N and Petrov K I 1975 *Russ. J. Inorg. Chem.* **20** 874
[48] Kol'tsova T N 2001 *Inorg. Mater.* **37** 1175
[49] Sumithra S and Umarji A M 2005 *Mater. Res. Bull.* **40** 167
[50] Duan N, Kamerwari U and Sleight A W 1999 *J. Am. Chem. Soc.* **121** 10432
[51] Varga T, unpublished
[52] Largarec K and Desgreniers S 1994–97 *Computer Code Simplified Image Plate Analysis* (Ottawa, ON: University of Ottawa)
[53] JADE 1995–2005 *Computer Code for XRD Pattern Processing* (Livermore, CA: Materials Data, Inc.)
[54] Larson A C and Von Dreele R B 2000 *Computer Code General Structural Analysis System* (Los Alamos, NM: Los Alamos National Laboratory)
[55] Zhao J 1998 *Computer Code Calibration* (Johannesburg-Gauteng: University of Witwatersrand)
[56] Birch F 1986 *J. Geophys. Res.* B **91** 4949
[57] Brown J M 1999 *J. Appl. Phys.* **86** 5801
[58] Mueller H J, Schilling F R, Lauterjung J and Lathe C 2003 *Eur. J. Mineral.* **15** 865
[59] Abrahams S C and Bernstein J L 1966 *J. Chem. Phys.* **45** 2745
[60] Evans J S O and Mary T A 2000 *Int. J. Inorg. Mater.* **2** 143
[61] Birch F 1947 *Phys. Rev.* **71** 809
[62] Angel R J 2001 *Computer Code EOS-FIT* (Blacksburg, VA: Virginia Tech)
[63] Sleight A W and Brixner L H 1973 *J. Solid State Chem.* **7** 172
[64] Evans J S O, Mary T A and Sleight A W 1997 *J. Solid State Chem.* **133** 580
[65] Evans J S O, Mary T A and Sleight A W 1998 *J. Solid State Chem.* **137** 148
[66] Imanaka N, Hiraiwa M, Adachi G, Dabkowska H and Dabkowski A 2000 *J. Cryst. Growth* **220** 176
[67] Sikka S K 2004 *J. Phys.: Condens. Matter* **16** S1033